CCSD(T) Study of CD_3-O-CD_3 and CH_3-O-CD_3 Far-Infrared Spectra

M. L. Senent

R. Dominguez-Gomez

M. Carvajal

M. Villa

ABSTRACT: From a vibrationally corrected 3D potential energy surface determined with highly correlated ab initio calculations (CCSD(T)), the lowest vibrational energies of two dimethyl-ether isotopologues, $^{12}CH_3-^{16}O-^{12}CD_3$ (DME-d_3) and $^{12}CD_3-^{16}O-^{12}CD_3$ (DME-d_6), are computed variationally. The levels that can be populated at very low temperatures correspond to the COC-bending and the two methyl torsional modes. Molecular symmetry groups are used for the classification of levels and torsional splittings. DME-d_6 belongs to the G_{36} group, as the most abundant isotopologue $^{12}CH_3-^{16}O-^{12}CH_3$ (DME-h_6), while DME-d_3 is a G_{18} species. Previous assignments of experimental Raman and far-infrared spectra are discussed from an effective Hamiltonian obtained after refining the ab initio parameters. Because a good agreement between calculated and experimental transition frequencies is reached, new assignments are proposed for various combination bands corresponding to the two deuterated isotopologues and for the 020 → 030 transition of DME-d_6. Vibrationally corrected potential energy barriers, structural parameters, and anharmonic spectroscopic parameters are provided. For the $3N - 9$ neglected vibrational modes, harmonic and anharmonic fundamental frequencies are obtained using second-order perturbation theory by means of CCSD and MP2 force fields. Fermi resonances between the COC-bending and the torsional modes modify DME-d_3 intensities and the band positions of the torsional overtones.

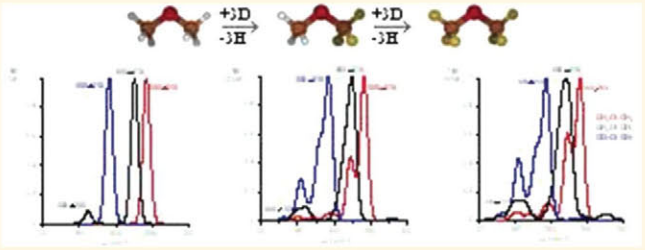

INTRODUCTION

It is expected that DME isotopologues are relevant interstellar molecular species because DME represents the most abundant ether in the gas-phase extraterrestrial sources.[1] Since its first detection in emission from the Orion Nebula by Snyder et al. in 1974,[2] it represents a common molecule of astrophysical surveys.[3] However, surveys contain many spectral lines whose identification requires the completion of molecular catalogs.[4] Spectral lines come from sources where very well known molecules coexist with uncharacterized species and with already detected ones that are not fully described. In the case of DME, only the vibrational ground state and three fundamental stretching bands of the most abundant isotopologue have been explored,[3−9] although presumably some of their isotopologues containing either deuterium or ^{13}C could be identified in the interstellar medium. Many facts concerning their abundances in hot core regions are expected to be clarified with the new observatory ALMA, which was devised as a key instrument for their studies.[10] The temperature of these regions varies from 100 to 300 K, which allows one to contain vibrationally excited molecules.

From the theoretical point of view, DME is a nonrigid molecule whose potential energy surface (PES) contains nine minima[11−13] that split the vibrational term values. The two torsional modes present very low energy levels that can be populated at low temperatures, such as those of hot cores. For this reason, a suitable astrophysical modeling also requires information relative to the excited torsional levels, and hence, new spectral measurements are necessary. Besides, highly correlated theoretical methods could be very helpful in the

assignment task. Ab initio calculations can discern the role played by the COC-bending mode in the torsional spectra.[11] It is well-known that in DME-h_6,[11] Fermi interactions shift the torsional overtones significantly. As isotopic substitution varies the relative positions of bands, the strength of the Fermi resonances could also change.

Recently, an accurate three-dimensional potential energy surface (3D-PES) of dimethyl-ether (DME) was computed for the analysis of torsional band structures.[11] The 3D-PES depending on the COC-bending and the two methyl group torsional coordinates was calculated using highly correlated ab initio methods (CCSD and CCSD(T)). In ref 11, information about DME minimum-energy geometries, potential energy barriers, and anharmonic spectroscopic fundamental frequencies are provided.

From the recently computed DME 3D-PES,[11] vibrational energy levels and transitions corresponding to the IR and Raman spectra in the far-infrared region were determined successfully for the most abundant isotopologue $^{12}CH_3-^{16}O-^{12}CH_3$ (DME-h_6). The main objective of the previous work was to produce and to test a tool, the 3D-PES, adequate for further interpretations of the unexplored spectra of the DME isotopologues. The application to DME-h_6 represented the first test of accuracy.

In the present paper, we analyze two DME isotopologues containing deuterium, $^{12}CD_3-^{16}O-^{12}CD_3$ (DME-d_6) and $^{12}CH_3-^{16}O-^{12}CD_3$ (DME-d_3), of which far-infrared and microwave spectra were recorded by Groner and Durig in the 1970s.[5,14] Here, we review the former spectral assignments from a different point of view, the one provided by accurate ab initio calculations. In addition, as some experimental data are available, this work represents a new test to scrutinize the accuracy of our CCSD(T) 3D-PES.[11] The precision of our PES needs to be well-defined before using it for helping assignments of the unexplored DME isotopologues.

In previous papers,[11,13] we showed that Fermi interactions force us to use a 3D model to obtain accurate band structures. In the present paper, we have applied it for the study of two deuterated species using our previously calculated 3D-PES and our full-dimensional anharmonic force field.[11] Some vibrational corrections, such as the zero-point vibrational energy correction, are first determined because they are mass-dependent. Thus, in the first section, we discuss the new ab initio results and some theoretical aspects such as the symmetry classification of the isotopic species. In the second section, we present the spectroscopic parameters and a discussion about the assignments and intensities of the vibrational transitions for both deuterated species. We provide MP2 harmonic and harmonic fundamentals and many spectroscopic parameters determined using second-order perturbation theory as well as CCSD harmonic fundamentals for the 21 vibrational modes. The levels of the three low-lying frequency modes (the COC-bending and the clockwise−clockwise and clockwise−counterclockwise torsional modes) are calculated variationally. From the energy levels, we discuss previous assignments, and we propose interpretations for unassigned transitions.

THEORETICAL ASPECTS AND COMPUTATIONAL DETAILS

In previous papers,[11−13] we studied a three-dimensional (3D) model for understanding of DME far-infrared spectra. Then, the 3D Hamiltonian can be defined as

$$\hat{H}_{3D} = -\sum_{i}^{3}\sum_{j}^{3}\left(\frac{\partial}{\partial q_j}\right)B_{ij}\left(\frac{\partial}{\partial q_i}\right) + V(\alpha, \theta_1, \theta_2) + V'(\alpha, \theta_1, \theta_2) + V^{ZPVE}(\alpha, \theta_1, \theta_2) \qquad i, j = \alpha, \theta_1, \theta_2 \tag{1}$$

where α, θ_1, and θ_2 are the three independent coordinates, the COC-bending and the two torsional coordinates (for their definitions, see Figure 1). In our previous paper,[11] we detailed

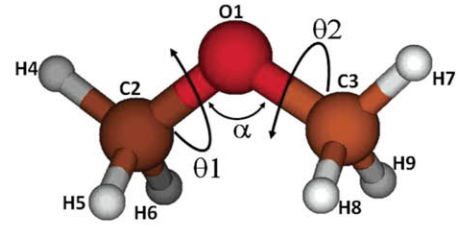

Figure 1. DME at the equilibrium geometry. Independent coordinates α, θ_1, and θ_2.

how to obtain θ_1 and θ_2 using a totally symmetric linear combination of the H4C2O1C3, H5C2O1C3, and H6C2O1C3 (or H7C2O1C3, H8C2O1C3, and H9C2O1C3) dihedral angles.

In eq 1, the first term that depends on the B_{ij} parameters (the G matrix elements in cm^{-1}) is a 3D kinetic energy operator T_{3D}; $V(\alpha,\theta_1,\theta_2)$, $V'(\alpha,\theta_1,\theta_2)$, and $V^{ZPVE}(\alpha,\theta_1,\theta_2)$ represent the PES, the "Podolsky pseudopotential", and the zero-point vibrational energy correction, respectively.[15,16]

The aim of the present paper is the study of two deuterated isotopologues DME-d_6 and DME-d_3. DME-d_6 can be classified in the G_{36} molecular symmetry group (MSG), such as the most abundant species DME-h_6.[12,13,15−18] G_{36} contains nine irreducible representations: four nondegenerate A_1, A_2, A_3, and A_4, four doubly degenerate E_1, E_2, E_3, and E_4, and one four-fold degenerate G. On the other hand, DME-d_3 shows G_{18} symmetry.[14,18] The G_{18} MSG contains two nondegenerate irreducible representations and four doubly degenerate ones. In the table below, the correlation between G_{36} and G_{18} symmetries is established (see also ref 19).

G_{36}	G_{18}	G_{36}	G_{18}	G_{36}	G_{18}	G_{36}	G_{18}
A_1	} A_1	E_{1a}	} E_{3a}	E_{1b}	} E_{3b}	G_a	} E_1
A_4		E_{2a}		E_{2b}		G_b	
A_2	} A_2	E_{3a}	} E_{4a}	E_{3b}	} E_{4b}	G_c	} E_2
A_3		E_{4a}		E_{4b}		G_d	

where the indexes a, b, c and d in the stand for each component of a degenerate irreducible representation.

The $V(\alpha,\theta_1,\theta_2)$ PES is isotopically invariant. For this reason, in this paper, we employ the very accurate PES calculated for the DME-h_6 isotopologue study.[11] The PES was determined at the ground electronic state from the energies of 126 molecular conformations defined for selected values of the independent coordinates covering the broad region around the minima. The remaining 18 coordinates were allowed to be relaxed in each molecular conformation. To obtain realistic spectroscopic parameters, we have searched for a correct definition of the torsional coordinates. Energies and molecular geometries were determined with coupled cluster theory using both single and double substitutions.[20] To improve the energies, single-point calculations were performed adding triple excitations non-iteratively (CCSD(T)) on the CCSD geometries.[21] Long-range

effects such as the intramolecular nonbonding interactions are well-described because the augmented aug-cc-pVTZ basis set was employed in all of the computations.[22] We used the following analytical expression for the PES:

$$V(\alpha, \theta_1, \theta_2) = \sum_{M=0}^{4}\sum_{N=0}^{2}\sum_{L=0}^{2}[A_{MNL}\alpha^M \cos(3N\theta_1) \cos(3L\theta_2)] + \sum_{M=0}[B_{M11}\alpha^M \sin(3\theta_1) \sin(3\theta_2) \quad (2)$$

This triple series transforms as the totally symmetric representation of the G_{36} MSG if $A_{MNL} = A_{MLN}$. This PES shows nine equivalent minima separated by relatively low potential barriers.

On the other hand, $V'(\alpha,\theta_1,\theta_2)$, $V^{ZPVE}(\alpha,\theta_1,\theta_2)$, and the B_{ij} functions depend on the isotopic masses. The V' pseudopotential as well as the kinetic energy matrix elements B_{ij} are calculated for the 126 geometries using the MATRIZG subroutine implemented in ENEDIM (see ref 11). The 126 values of each function are fitted to symmetry-adapted triple series that carry the totally symmetric representations of the G_{36} and G_{18} groups.

For each geometry, $V^{ZPVE}(\alpha,\theta_1,\theta_2)$ is determined from the MP2/aug-cc-pVTZ harmonic frequencies ω_i:

$$E^{ZPVE} = \sum_{i=n+1}^{i=3N-6}\frac{\omega_i}{2} \quad (3)$$

where the sum neglects the two torsional and the COC-bending modes ($n = 3$). The vibrational MP2 correction of the 3D-PES is determined in the present paper for each isotopologue using Gaussian 09[23] and 126 geometries optimized at the MP2/aug-cc-pVTZ level. Individual values of the ZPVE correction corresponding to the 126 conformations are fitted to a totally symmetric series similar to eq 2:

$$V^{ZPVE}(\alpha, \theta_1, \theta_2) = \sum_{M=0}^{4}\sum_{N=0}^{2}\sum_{L=0}^{2}[A_{MNL}^{ZPVE}\alpha^M \cos(3N\theta_1) \cos(3L\theta_2)] + \sum_{M=0}B_{M11}^{ZPVE}\alpha^M \sin(3\theta_1) \sin(3\theta_2) \quad (4)$$

where $A_{MNL} = A_{MLN}$ for DME-d_6 and $A_{MNL} \neq A_{MLN}$ for DME-d_3.

The 3D Hamiltonian is solved variationally using ENEDIM code.[24a] As a basis set, we use symmetry-adapted eigenvectors derived from the product of the double Fourier series for the torsional angles and the solutions of the harmonic oscillator for the COC-bending angle. The convergence of the levels is reached only too well for the accuracy of the available experimental data with a Hamiltonian matrix of dimension 28350 (45 × 45 torsional functions and 14 bending harmonic functions). For DME-d_6, the matrix factorizes into 16 blocks whose dimensions are 896 (A_1), 784 (A_2 and A_3), 686(A_4), 1680 (E_1 and E_3), 1470 (E_2 and E_4), and 3150 (G); for DME-d_3, the dimensions are 1582 (A_1), 1568 (A_2), and 3150 (E_1, E_2, E_3, and E_4). This basis set is larger than the one used in our previous paper for DME-h_6[11] because we provide excited levels up to $\nu = 5$.

Infrared intensities in the absorption spectrum for the c-type transitions, which shows strong Q-branches, are determined by the equation:[12,17]

$$I_R^c = \frac{g}{3B}(E_f - E_i)(C_i - C_f)\left\langle \phi_f \left| \frac{\mu_c}{Re} \right| \phi_i \right\rangle^2 \quad (5)$$

In this expression, (E_i and E_f) and (ϕ_i and ϕ_f) are the energies and the wave functions of initial and final levels involved in the transition. Coefficients C_i and C_f are the Boltzmann fractional populations of the two states at a given temperature T, e is the electron charge, g represents the nuclear spin statistical weight, R is the average distance among the hydrogen atoms in the methyl top and the internal rotation axis, and B is the average internal rotation constants (for definitions, see ref 12; $B = (B_{\alpha\alpha}B_{\theta1\theta1}B_{\theta2\theta2})^{1/3}$); μ_c is the c-principal axis (out-of-plane) component of the dipole moment. The dipole moment components are calculated for the previously mentioned 126 geometries with the MP2/aug-cc-pVTZ level with the Gaussian package.[23] Individual values of μ_c are fitted to a series that carries a A_2 symmetry for both isotopologues, DME-d_6 and DME-d_3, with G_{36} and G_{18} molecular symmetry groups, respectively. The symmetry loss of DME coming from the partial deuteration in DME-d_3 has an effect on the symmetry properties of the a and b components of the dipole moment but not on the out-of-plane component. Selection rules for DME-d_6 are defined in refs 12 and 17. For DME-d_3, they can be deduced using the correlation table.

To determine spectroscopic parameters corresponding to the remaining $3N - 9$ coordinates, the full-dimensional anharmonic spectroscopic analysis was performed with second-order perturbation theory (PT2) implemented in FIT-ESPEC.[24b] The starting point was a CCSD quadratic force field and cubic and quartic force fields determined with second-order Möller–Plesset theory (MP2).[11]

■ RESULTS AND DISCUSSION

The DME structure and the 3D-PES are discussed in ref 11. In the present paper, we provide some mass-dependent properties of both deuterated DME species under study. Tables 1 and 2 summarize relevant results of the full-dimensional anharmonic analysis for both isotopologues performed using second-order perturbation theory. Table 3 shows their rotational constants and their effective torsional barriers. Table 4 displays the significant parameters of the torsion–torsion-bending Hamiltonian, and Tables 5–7 contain the relative intensities and the vibrational transition frequencies calculated variationally. Relative intensities are determined at room temperature (300 K), at a very low temperature (10K) feasible in the interstellar medium (ISM), and at 200 K, which represents an average temperature of hot cores. Figure 2 allows comparison of the FIR spectrum at these three temperatures.

Full-Dimensional Anharmonic Analysis. Although accurate calculations of torsional energies and splittings demand a variational treatment, the PT2 full-dimensional anharmonic analysis supplies information about the neglected vibrational modes and the first approximate values for the COC-bending and torsional fundamental frequencies (see Tables 1 and 2). This analysis allows us to predict interactions between large and small vibrational modes and to validate the 3D model.

Then, we use the CCSD/aug-cc-pVTZ harmonic force field and the MP2/aug-cc-pVTZ anharmonic force field, determined in ref 11, to obtain DME-h_6, DME-d_6, and DME-d_3 fundamental bands (see Table 1) and rotational and quartic centrifugal distortion constants (see Table 2). In Table 1, the vibrational frequencies are classified using the irreducible representations of the C_{2v} (DME-h_6 and DME-d_6) and C_s

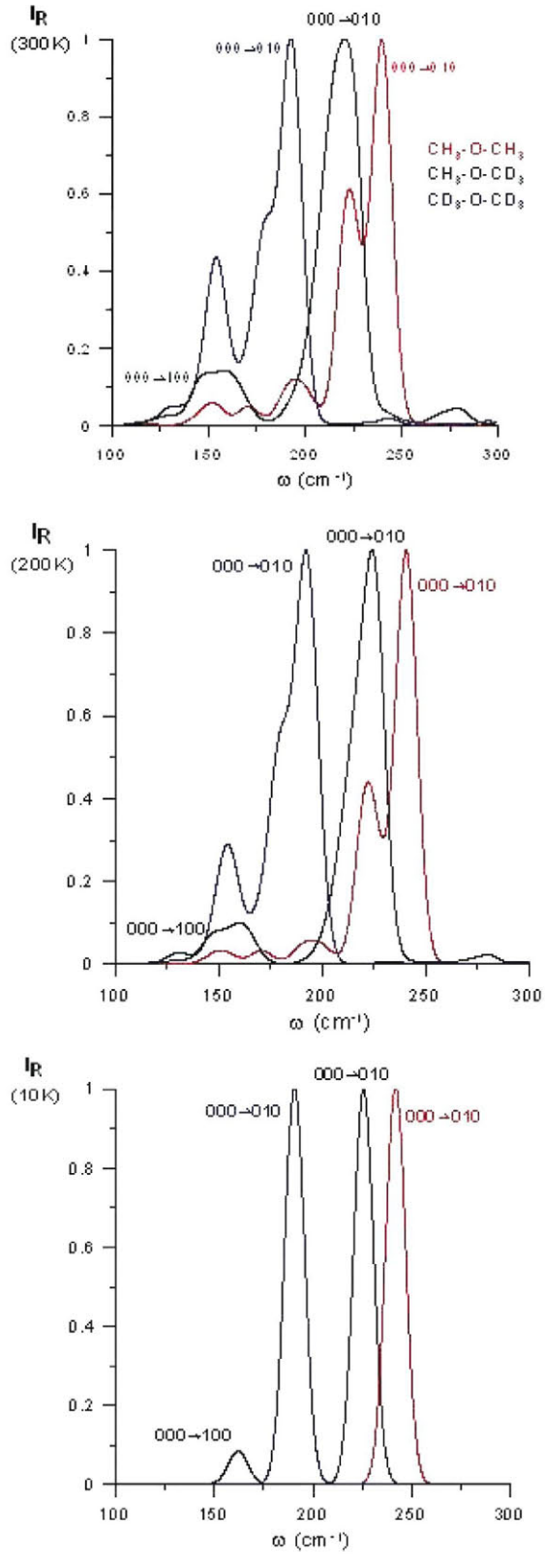

Figure 2. Simulation of the FIR spectra of DME-h_6, DME-d_3, and DME-d_6 species at 300, 200, and 10 K.

(DME-d_3) point groups. Isotopic effects can be derived by comparing the results of the deuterated species with those of DME-h_6. Vibrational bands displaced more than 10 cm^{-1} by Fermi resonances are highlighted in boldface. They correspond to the H-stretching modes. In Table 2, the rotational constants are compared with those of Durig et al.[5] that were fitted from the experimental spectra. Observed centrifugal distortion constants come from millimeter spectroscopy.[3]

For the COC-bending mode, the CCSD harmonic frequencies are calculated with values ν_7 = 421 cm^{-1} (DME-h_6), ν_7 = 355 cm^{-1} (DME-d_6), and ν_{13} = 387 cm^{-1} (DME-d_3). They present differences of 4, 3, and 4 cm^{-1} with respect the MP2 harmonic ones, respectively. MP2 anharmonic band centers are found to be ν_7 = 410 cm^{-1} (DME-h_6), ν_7 = 335 cm^{-1} (DME-d_6), and ν_{13} = 368 cm^{-1} (DME-d_3) at −2, −6, and −5 cm^{-1} from the experimental values (ν_7 = 412 cm^{-1} (DME-h_6), ν_7 = 341 cm^{-1} (DME-d_6), and ν_{13} = 373 cm^{-1} (DME-d_3)[14]). PT2 and the MP2 force field reproduce accurately the band position shifts when isotopic substitutions with deuterium are carried out.

For the computed torsional frequencies, it is noticed that electron correlation (CCSD level of theory) decreases their values with respect to those obtained with a MP2 force field. MP2 anharmonic fundamental frequencies are calculated to be ν_{15} = 246 cm^{-1} and ν_{11} = 202 cm^{-1} (DME-h_6), ν_{15} = 192 cm^{-1} and ν_{11} = 148 cm^{-1} (DME-d_6), and ν_{20} = 225 cm^{-1} and ν_{21} = 172 cm^{-1} (DME-d_3). The corresponding experimental values were observed at ν_{15} = 241.0 cm^{-1} (DME-h_6), ν_{15} = 188.6 cm^{-1} (DME-d_6), and ν_{20} = 223.9 cm^{-1} and ν_{21} = 162.0 cm^{-1} (DME-d_3).[14]

Table 2 also shows predicted Fermi displacements of the torsional and bending levels. Strong interactions between torsional overtones and the COC-bending fundamental are expected for the three isotopic varieties. A negligible effect on the DME-d_6 $2\nu_{11}$ overtone is obtained.

Raman and Far-Infrared Spectra. The lowest vibrational energy levels are calculated by solving variationally the 3D Hamiltonian (eq 1). For both DME-d_6 and DME-d_3, the levels split by a tunneling effect in the potential barriers into nine components corresponding to the nine wells of the PES. For DME-d_6, splitting components transform as the A_i, E_i (i = 1−4), and G symmetry representations, whereas for DME-d_3, they transform as A_1, A_2, E_1, E_2, E_3, and E_4. For both isotopologues, below 800 cm^{-1}, splitting energy differences are in general lower than 0.1 cm^{-1}.

Table 3 shows the effective torsional one-dimensional (1D) and two-dimensional (2D) barriers V_{060} and V_{6060}, which stand for the energy differences $V_{060} = V^{ef}(\alpha,0,60) - V^{ef}(\alpha,0,0)$ and $V_{6060} = V^{ef}(\alpha,60,60) - V^{ef}(\alpha,0,0)$ for $\alpha = 0°$, respectively. The effective potential V^{ef} has mass-dependent parameters because it depends on vibrationally corrected energies ($V^{ef} = V + V^{ZPVE} + V'$). Whereas V' is negligible, the ZPVE correction is important. Without ZPVE, V_{060} = 921 cm^{-1} and V_{6060} = 1966 cm^{-1}. The difference $V_{6060} - 2V_{060}$ measures the interaction between the two torsional modes, which is larger for DME-d_3, the most asymmetric isotopologue. The effect of isotopic substitution on torsional frequencies and parameters has been discussed previously in our papers about acetic acid isomers.[25−27] By comparing alike molecules containing methyl groups, it is evident that the relative positions of V_{6060} and V_{060} clearly depend on molecular symmetry and geometrical parameters.[12,17,28,29] In DME, the two methyl groups interact strongly. This interaction is a function of the COC angle through the nonbonding interactions between H atoms of different methyl groups.[11]

In Table 4, the most significant parameters of the effective PES V^{ef} are shown ($V^{ef}(\alpha,\theta_1,\theta_2) = V(\alpha,\theta_1,\theta_2) + V'(\alpha,\theta_1,\theta_2) + V^{ZPVE}(\alpha,\theta_1,\theta_2)$) (eq 2). The PES was obtained by fitting the

Table 1. Harmonic (ω) and Anharmonic (ν) Fundamental Frequencies of DME (in cm^{-1})[a]

		DME-h_6			DME-d_6					DME-d_3		
		CCSD	MP2		CCSD	MP2				CCSD	MP2	
C_{2v}	mode	ω	ω	ν^b	ω	ω	ν^b	C_s	mode	ω	ω	ν^b
A_1	υ_1	3147	3179	3050	2333	2357	2298	A′	υ_1	3146	3179	3006
	υ_2	3011	3024	**2827**	2162	2170	**2061**		υ_2	3006	3021	2842
	υ_3	1537	1533	1490	1191	1173	1146		υ_3	2331	2356	**2256**
	υ_4	1511	1498	1461	1110	1106	1080		υ_4	2157	2167	2071
	υ_5	1291	1275	1244	1082	1068	1048		υ_5	1528	1525	1479
	υ_6	971	958	931	853	848	831		υ_6	1496	1484	1452
	υ_7	421	417	405	355	352	335		υ_7	1256	1240	1216
B_2	υ_{16}	3145	3178	3045	2329	2354	2279		υ_8	1207	1187	1155
	υ_{17}	3002	3019	2898	2153	2164	**2066**		υ_9	1147	1134	1108
	υ_{18}	1522	1519	1471	1215	1192	1161		υ_{10}	1105	1102	1073
	υ_{19}	1478	1467	1434	1101	1099	1073		υ_{11}	976	967	946
	υ_{20}	1231	1211	1176	1090	1084	1063		υ_{12}	886	880	859
	υ_{21}	1139	1131	1105	878	872	860		υ_{13}	387	383	368
B_1	υ_{12}	3055	3082	2950	2264	2285	**2226**	A″	υ_{14}	3057	3086	2966
	υ_{13}	1521	1518	1470	1101	1098	1074		υ_{15}	2267	2289	**2188**
	υ_{14}	1212	1201	1173	957	949	930		υ_{16}	1516	1512	1455
	υ_{15}	252	260	246	195	200	192		υ_{17}	1197	1189	1160
A_2	υ_8	3059	3090	**2978**	2269	2293	**2230**		υ_{18}	1096	1093	1073
	υ_9	1511	1507	1461	1092	1089	1068		υ_{19}	925	918	902
	υ_{10}	1180	1173	1151	895	890	876		υ_{20}	233	240	225
	υ_{11}	202	210	202	144	150	148		υ_{21}	165	171	172

[a]The DME-h_6 and DME-d_6 symmetry labels of the vibrational modes are mixed up deliberately so that the C_{2v} and C_s irreducible representations are kept matched. [b]Fermi interactions are included in the anharmonic fundamental frequencies (emphasized in boldface when the Fermi displacement is bigger than 10 cm^{-1}).

Table 2. Predicted Spectroscopic Properties Using Second-Order Perturbation Theory Calculated with MP2/aug-cc-pVTZ

	DME-h_6		DME-d_6		DME-d_3	
			Fermi Displacements of Torsional and Bending Bands (in cm^{-1})			
$2\nu_{11}$	401 → 398		$2\nu_{11}$		$2\nu_{21}$	339 → 338
$2\nu_{15}$	491 → 498		$2\nu_{15}$	386 → 394	$2\nu_{20}$	442 → 448
ν_7	410 → 405		ν_7	343 → 335	ν_{13}	375 → 368
	calc.	obs.[3,5]	calc.	obs.[5]	calc.	obs.[5]
			Rotational Constants (in MHz)			
A_e	38549.07		25673.99		30820.44	
B_e	10192.86		7570.32		8743.48	
C_e	8974.20		6857.41		7818.65	
A_0	38405.04	38789.66	25651.85		30782.49	30914.26
B_0	10038.45	10059.91	7672.77		8872.32	8639.12
C_0	8851.91	8880.58	6947.03		7927.21	7741.16
$A_{\nu7}$	39030.36		25654.97		30797.20	
$B_{\nu7}$	10014.68		7719.57		8931.87	
$C_{\nu7}$	8817.27		6958.12		7939.91	
$A_{\nu11}$	38417.92	38835.24	25114.86	25707.98	30152.36	30920.35
$B_{\nu11}$	10009.19	10029.43	7650.78	7469.85	8852.36	8615.91
$C_{\nu11}$	8828.64	8862.77	6935.73	6781.73	7922.92	7727.50
$A_{\nu15}$	38419.36	38803.18	25148.61	25677.36	30025.11	30918.02
$B_{\nu15}$	9967.78	10004.48	7676.05	7457.18	8875.07	8599.40
$C_{\nu15}$	8824.86	8849.84	6968.56	6774.82	7943.98	7717.67
			Centrifugal Distortion Constants (in MHz)			
Δ_J	0.0095	0.0091	0.0049		0.0067	
Δ_K	0.3346	0.3420	0.0686		0.1403	
Δ_{JK}	−0.0313	−0.0269	0.0001		−0.0068	
δ_J	0.0019	0.0018	0.0008		0.0012	
δ_K	−0.0087	−0.0138	−0.0123		−0.0163	

Table 3. CCSD(T) Equilibrium Rotational Constants (in MHz) and Vibrationally Corrected Potential Energy Barriers (in cm^{-1})

	DME-h_6	DME-d_6	DME-d_3
A_e	38973.4024	25853.98	31085.50
B_e	10145.2871	7533.13	8701.58
C_e	8961.8951	6841.78	7804.12
$V_{060}(\alpha=0°)$	939	918	923
$V_{6060}(\alpha=0°)$	1984	1948	1966
$V_{6060} - 2V_{060}$	106	108	120

Table 4. More Significant Parameters of the Torsion–Torsion-Bending-Effective Hamiltonian (in cm^{-1})[a]

	DME-d_6[b]	DME-d_6[c] (adjusted)	DME-d_3[b]	DME-d_3[c] (adjusted)
	Potential Energy Surface ($V^{ef} = V + V' + V^{ZPVE}$)			
A_{200}[d]	10.482	9.540	10.515	9.780
A_{010}	−488.249	−488.249	−492.163	−487.163
A_{001}	−488.249	−488.249	−492.164	−487.164
A_{011}	27.200	27.200	29.168	29.168
B_{011}	−15.525	−4.525	−15.782	−15.782
	Kinetic Energy Parameters			
$A_{000}(B_{\theta 1\theta 1})$	3.7986	3.7986	6.5130	6.5130
$A_{000}(B_{\theta 2\theta 2})$	3.7986	3.7986	4.0191	4.0191
$A_{000}(B_{\alpha\alpha})$	1.2711	1.2107	1.4498	1.3698
$A_{000}(B_{\theta 1\theta 2})$	−0.9716	−0.9716	−1.0856	−1.0856
γ[e]	4.467	4.518	4.612	4.653
Factor[f]	0.000	4.75	0.0	3.65

[a]The potential and kinetic coefficients are defined with the expansion of eq 2. [b]Parameter values obtained with the ab initio CCSD(T)/aug-cc-pVTZ level of theory. [c]Parameter values obtained after carrying out the adjustment of the Hamiltonian detailed in the text. [d]A_{200} in cm^{-1}/degrees^2 [e]The harmonic oscillator parameter $\gamma^4 = A_{200}/A_{000}(B_{\alpha\alpha})$ of the COC-bending wave function. [f]Factor (eq 6) for DME-h_6 = 1.95.[11]

126 energies to a symmetry-adapted function.[11] As the 126 conformations were selected taking into consideration energetic and symmetry criteria, the fit is very accurate ($R^2 = 1$, $\sigma = 0.62$ cm^{-1}). A_{200} represents the harmonic term of the 1D COC-bending potential; A_{010} and A_{001} depend directly on the torsional barrier height, V_{060}, and A_{011} and B_{011} are interaction term coefficients between both torsional modes. B_{011}, is the sin $3\theta_1 \sin 3\theta_2$ coefficient that collects the energy difference between the two torsional modes, clockwise–clockwise and clockwise–counterclockwise. In the same table, some independent coefficients of the kinetic energy parameters are presented as the γ parameter of the harmonic oscillator solutions and the Factor parameters used for the PES refinement (see below). The Factor values are taken as zero for pure ab initio cases without any further refinement.

In Tables 5–7, calculated Raman and FIR transitions are compared with previously observed and assigned bands,[14] which are in boldface. IR spectra at 300, 200, and 10 K are also shown and represented in Figure.2 for DME-h_6, DME-d_6, and DME-d_3. The intensities are presented relative to the strongest band of each isotopologue. In general, there is a good agreement between calculated and observed band positions for all isotopologues, especially for DME-d_3.

The effect of the ZPVE correction on the fundamental transitions is very small. This correction displaces the bending fundamental less than 1 cm^{-1} and the torsional ones less than 4 cm^{-1}.

In our previous paper,[11] we showed that the first source of deviations between observed and ab initio data is our definition of the COC-bending. The accuracy was better for the torsional transitions than that for bending ones. When we identified the COC-bending vibrational coordinate, which depends on $3N - 6$ internal coordinates, with the COC angle α, the contribution of the in-plane HCO angles was missing. This neglect brought in an error that is larger for heavy deuterated species. For DME-h_6,[11] we determined the frequency with a residual of 9 cm^{-1} for the vibrational mode ν_7. For DME-d_6 and DME-d_3, we calculated the COC-bending fundamental frequencies at 358.1 cm^{-1} (DME-d_6) and 396.2 cm^{-1} (DME-d_3), whereas their experimental bands, observed in the Raman spectra, lie at 341.0 and 373.0 cm^{-1}.[14]

Therefore, to explore the concrete source of deviations, we have adjusted the PES defining a new α' coordinate

$$\alpha' = \alpha + \text{Factor}*\alpha/100 \quad (6)$$

which corrects the contribution of the internal α angle to the normal COC-bending coordinate α'.

Hence, the $B_{\alpha\alpha}$ kinetic parameter also needs to be corrected in all of the conformations (e.g., $B_{\alpha\alpha}' = B_{\alpha\alpha} - \text{Factor}*B_{\alpha\alpha}/100$).

By using the set of α', θ_1, θ_2 coordinates instead of the original set α, θ_1, θ_2 for the fitting of the CCSD(T) electronic energies, a new PES is obtained where A_{200} is clearly modified. For DME-h_6, DME-d_3, and DME-d_6 species, Factor needs to be 1.954,[11] 3.654, and 4.754, which represent coordinate corrections lower than 2, 4, and 5%, respectively. The new fitting surface places the COC-bending fundamental frequencies at 341.1 cm^{-1} (DME-d_6) and 373.1 cm^{-1} (DME-d_3), very close to the observed values (341.0 and 373.0 cm^{-1}, respectively).

Once a new PES is obtained after replacing α by α', a single coefficient is also shifted for each isotopologue, B_{011} for DME-d_6 and A_{010} (keeping $A_{010} = A_{001}$ for the potential term V) for DME-d_3, to obtain very accurate torsional energies. Thus, the definitive adjusted PES (V^{ADJ}) reproduces accurately both bending and torsional frequencies. In Table 4, the most significant pure ab initio parameters of the Hamiltonian are compared with those obtained after refinement for the species under study. As the adjusted surfaces lead to very accurate energies, they can be used as starting points for future assignments and fittings of new experimental values.

DME-d_6. For DME-d_6, only a fundamental transition (ν_{15}, 000 →010) is IR-active. CCSD(T) calculations place it at 192.8 cm^{-1}, close to experimental value of 188.6 cm^{-1}. Adjustment displaces it to 190.6 cm^{-1}. Inverted anharmonicities of ν_{15} are calculated and observed. Frequencies corresponding to the $0,n,0 \rightarrow 0,n+1,0$ series increase with n. This fact is a distinctive mark of the fully deuterated species. Anharmonic effects are shown to be really strong for the transition 010 → 020, observed at 195.3 cm^{-1} and calculated at 194.8 cm^{-1}, because the 020 level (385.4 + E^{ZPVE} cm^{-1}) is strongly displaced by the COC-bending fundamental band (ν_7 = 341.0 + E^{ZPVE} cm^{-1}) through a Fermi resonance.

Experimental spectral lines were assigned by keeping the labeling of the Raman and the infrared transition lines and of the microwave data predictions [ref 14 and references therein]. Whereas the experimental spectra present a complex band structure, only seven Raman and six infrared bands were assigned. Our calculations confirm previous assignments; for example, transitions 100 → 110 and 200 → 210 observed at 179.1 and 168.7 cm^{-1} were calculated at 179.6 and 167.2 cm^{-1}

Table 5. Computed and Observed Far-Infrared and Raman Transitions of DME-d_6 (in cm^{-1})

	FIR						Raman			
	symm.	calc.[a]	adj.[b]	obs.[c]	$I_{R(300K)}$[d]		symm.	calc.[a]	adj.[b]	obs.[c]
000 → 010	$A_1 \rightarrow A_2$	192.8	190.6	**188.6**	0.57	000 → 001	$A_1 \rightarrow A_1$	358.1	341.1	**341.0**
	$G \rightarrow G$	192.8	190.6				$G \rightarrow G$	358.1	341.1	
	$E_1 \rightarrow E_1$	192.8	190.6				$E_1 \rightarrow E_1$	358.1	341.1	
	$E_3 \rightarrow E_4$	192.8	190.6				$E_3 \rightarrow E_3$	358.1	341.1	
010 → 020	$A_2 \rightarrow A_1$	205.3	194.8	**195.3**	0.86	000 → 020	$A_1 \rightarrow A_1$	398.1	385.4	**383.9**
	$G \rightarrow G$	205.3	194.8				$G \rightarrow G$	398.1	385.4	
	$E_1 \rightarrow E_1$	205.3	194.8				$E_1 \rightarrow E_1$	398.1	385.4	
	$E_4 \rightarrow E_3$	205.3	194.8				$E_3 \rightarrow E_3$	398.1	385.4	
020 → 030	$A_1 \rightarrow A_2$	201.9	195.1	**196.4**	0.4	010 → 030	$A_2 \rightarrow A_2$	407.2	389.9	**392.0**
	$G \rightarrow G$	201.9	195.1				$G \rightarrow G$	407.2	389.9	
	$E_1 \rightarrow E_1$	201.8	195.1				$E_1 \rightarrow E_1$	407.1	389.9	
	$E_3 \rightarrow E_4$	201.8	195.1				$E_4 \rightarrow E_4$	407.1	389.9	
030 → 040	$A_2 \rightarrow A_1$	204.4	195.9	**198.0**	0.19	020 → 040	$A_1 \rightarrow A_1$	406.3	391.0	**395.0**
	$G \rightarrow G$	204.4	195.5				$G \rightarrow G$	406.3	390.7	
	$E_1 \rightarrow E_1$	204.4	195.2				$E_1 \rightarrow E_1$	406.2	390.4	
	$E_4 \rightarrow E_3$	204.5	194.8				$E_3 \rightarrow E_3$	406.3	390.0	
200 → 210	$A_1 \rightarrow A_2$	169.3	167.2	**168.7**	0.25	030 → 050	$A_2 \rightarrow A_2$	408.4	391.5	**397.5**
	$G \rightarrow G$	169.3	167.2				$G \rightarrow G$	408.4	391.2	
	$E_1 \rightarrow E_1$	169.2	167.2				$E_1 \rightarrow E_1$	408.4	391.2	
	$E_3 \rightarrow E_4$	169.2	167.2				$E_4 \rightarrow E_4$	408.4	390.0	
100 → 110	$A_3 \rightarrow A_4$	181.7	179.6	**179.1**	1.0	100 → 120	$A_3 \rightarrow A_3$	388.5	369.8	**363.0**
	$G \rightarrow G$	181.7	179.6				$G \rightarrow G$	388.5	369.8	
	$E_2 \rightarrow E_2$	181.7	179.6				$E_2 \rightarrow E_2$	388.5	369.8	
	$E_3 \rightarrow E_4$	181.7	179.6				$E_3 \rightarrow E_3$	388.5	369.8	
110 → 120	$A_4 \rightarrow A_3$	206.8	190.3	*187.4*	0.57	000 → 200	$A_1 \rightarrow A_1$	283.5	286.3	**285.5**
	$G \rightarrow G$	206.8	190.3				$G \rightarrow G$	283.5	286.3	
	$E_2 \rightarrow E_2$	206.8	190.3				$E_1 \rightarrow E_1$	283.5	286.3	
	$E_4 \rightarrow E_3$	206.8	190.3				$E_3 \rightarrow E_3$	283.5	286.3	
001 → 011	$A_1 \rightarrow A_2$	171.9	174.8	*174.1*	0.27	100 → 300	$A_3 \rightarrow A_3$	275.4	277.5	–
	$G \rightarrow G$	171.9	174.8				$G \rightarrow G$	275.4	277.5	
	$E_1 \rightarrow E_1$	171.9	174.8				$E_2 \rightarrow E_2$	275.4	277.5	
	$E_3 \rightarrow E_4$	171.9	174.8				$E_3 \rightarrow E_3$	275.4	277.5	
						200 → 400	$A_1 \rightarrow A_1$	264.5	265.8	–
							$G \rightarrow G$	264.7	266.0	
							$E_1 \rightarrow E_1$	264.9	266.1	
							$E_3 \rightarrow E_3$	264.9	266.1	

[a]CCSD(T)/aug-cc-pVTZ frequencies. [b]Adjusted frequencies according to the text.[11] [c]In boldface are band energies assigned in ref 14; in italic are band assignments proposed in this work. [d]Relative intensity obtained from eq 5 for the infrared absorption spectrum.

with the adjusted PES (V^{ADJ}). At 300 K, 100 → 110 is the prominent band and reference for the relative intensities of other transition lines.

Calculated relative intensities at 300 K can help with the labeling of the levels. With the exception of the first sequence 010 → 020, the intensities of the 0,n,0 → 0,n+1,0 bands decreases with n. At ISM temperatures (10 K), the 000 → 010 transition presents the strongest observed Q-branch, which is the single observed one (see Figure 2). At 300 K, some transitions involving excited COC-bending levels and excited torsional levels also present significant intensities. The intensity enhancement can be related to the Fermi resonances. In 1977, Groner and Durig[14] suggested that an explanation of the unassigned patterns of bands could come from Fermi resonances.

Our calculations predict that the IR combination band 110 → 120 and the "hot" band 001 → 011 lie at 190.3 and 174.8 cm^{-1}, respectively. Those are relatively intense bands at 300 K. Therefore, they could be assigned to the bands observed at 187.4 and 174.1 cm^{-1}, respectively.[14] The Raman 100 → 310 and 200 → 400 overtones are predicted at 277.5 and around 266 cm^{-1}.

DME-d_3. The symmetry breaking produced by the partial deuteration of DME (DME-d_3) gives rise to a very complex spectrum. For this species, both torsional modes are infrared-active, although the largest intensities correspond to ν_{20} band series while ν_{21} band series are really weak. In fact, at 300 K, the strongest transition line corresponds to the ν_{20} fundamental. "Hot" transitions also show large intensities, and as for DME-d_6, the intensity enhancement can be related to the Fermi resonances.

In 1977, Groner and Durig[14] observed many lines, whereas only nine infrared transitions, three corresponding to the ν_{20} mode, four to the ν_{21} mode, and two combination bands, were assigned. From the CCSD(T) surface, the two fundamental frequencies were calculated at 227.0 and 163.0 cm^{-1}, very close to the experimental values of 223.9 and 162.0 cm^{-1}. The adjusted potential computed them at 225.5 and 162.0 cm^{-1}.

Generally, there is a very good agreement between calculations and observations. For example, the first sequence

Table 6. Computed and Observed Far-Infrared Transitions of DME-d_3 (in cm^{-1})

	symm.	calc.[a]	adj.[b]	obs.[c]	$I_{R(300K)}$[d]		symm.	calc.[a]	adj.[b]	obs.[c]	$I_{R(300K)}$[d]
		$\nu\ \nu'\ \nu'' \rightarrow \nu\ \nu'+1\ \nu''$						$\nu\ \nu'\ \nu'' \rightarrow \nu+1\ \nu'\ \nu''$			
000 → 010	$A_1 \rightarrow A_2$	227.0	225.6	**223.9**	1.0	000 → 100	$A_1 \rightarrow A_2$	163.0	162.0	**162.0**	0.07
	$E_1 \rightarrow E_1$	227.0	225.5				$E_1 \rightarrow E_1$	163.0	162.0		
	$E_2 \rightarrow E_2$	227.0	225.6				$E_2 \rightarrow E_2$	163.0	162.0		
	$E_3 \rightarrow E_3$	227.0	225.5				$E_3 \rightarrow E_3$	163.0	162.0		
	$E_4 \rightarrow E_4$	227.0	225.5				$E_4 \rightarrow E_4$	163.0	162.0		
010 → 020	$A_2 \rightarrow A_1$	221.7	217.0	**218.1**	0.57	100 → 200	$A_2 \rightarrow A_1$	155.2	154.1	**154.5**	0.06
	$E_1 \rightarrow E_1$	221.8	217.3				$E_1 \rightarrow E_1$	155.2	154.1		
	$E_2 \rightarrow E_2$	221.7	217.0				$E_2 \rightarrow E_2$	155.2	154.1		
	$E_3 \rightarrow E_3$	221.8	217.3				$E_3 \rightarrow E_3$	155.2	154.1		
	$E_4 \rightarrow E_4$	221.8	217.3				$E_4 \rightarrow E_4$	155.2	154.1		
020 → 030	$A_1 \rightarrow A_2$	222.6	215.1	*215.5*	0.22	200 → 300	$A_1 \rightarrow A_2$	145.3	144.1	**145.1**	0.04
	$E_1 \rightarrow E_1$	222.7	214.9				$E_1 \rightarrow E_1$	145.3	144.1		
	$E_2 \rightarrow E_2$	222.5	215.1				$E_2 \rightarrow E_2$	145.1	143.9		
	$E_3 \rightarrow E_3$	222.7	213.8				$E_3 \rightarrow E_3$	145.1	143.9		
	$E_4 \rightarrow E_4$	222.8	213.8				$E_4 \rightarrow E_4$	145.1	143.9		
030 → 040	$A_2 \rightarrow A_1$	216.1	210.3	**210.6**	0.06	300 → 400	$A_2 \rightarrow A_1$	131.2	130.0	**133.8**	0.02
	$E_1 \rightarrow E_1$	220.1	210.6				$E_1 \rightarrow E_1$	131.3	130.0		
	$E_2 \rightarrow E_2$	216.2	210.2				$E_2 \rightarrow E_2$	132.9	131.7		
	$E_3 \rightarrow E_3$	217.7	213.9				$E_3 \rightarrow E_3$	132.8	131.7		
	$E_4 \rightarrow E_4$	219.3	213.6				$E_4 \rightarrow E_4$	132.9	131.7		
						400 → 500	$A_1 \rightarrow A_2$	123.3	122.4	–	0.01
							$E_1 \rightarrow E_1$	123.2	127.3		
							$E_2 \rightarrow E_2$	111.0	116.9		
							$E_3 \rightarrow E_3$	111.1	126.1		
							$E_4 \rightarrow E_4$	111.0	126.1		
100 → 110	$A_2 \rightarrow A_1$	216.8	220.4	**221.8**	0.2	010 → 110	$A_2 \rightarrow A_1$	152.8	156.8	–	0.002
	$E_1 \rightarrow E_1$	216.9	220.5				$E_1 \rightarrow E_1$	152.9	157.0		
	$E_2 \rightarrow E_2$	216.8	220.4				$E_2 \rightarrow E_2$	152.8	156.8		
	$E_3 \rightarrow E_3$	216.9	220.5				$E_3 \rightarrow E_3$	152.9	157.0		
	$E_4 \rightarrow E4$	216.9	220.5				$E_4 \rightarrow E_4$	152.9	157.0		
110 → 120	$A_1 \rightarrow A_2$	214.6	205	**204.6**	0.1	110 → 210	$A_1 \rightarrow A_2$	149.7	157.4	–	0.002
	$E_1 \rightarrow E_1$	212.6	204.2				$E_1 \rightarrow E_1$	149.1	156.5		
	$E_2 \rightarrow E_2$	214.6	205				$E_2 \rightarrow E_2$	149.7	157.4		
	$E_3 \rightarrow E_3$	213.6	204.2				$E_3 \rightarrow E_3$	149.1	156.5		
	$E_4 \rightarrow E_4$	212.6	204.2				$E_4 \rightarrow E_4$	149.1	156.5		
001 → 011	$A_1 \rightarrow A_2$	204.7	211.4		0.12	001 → 101	$A_1 \rightarrow A_2$	159.2	152.1	–	0.01
	$E_1 \rightarrow E_1$	204.4	209.5	*209.8 or 211.4*			$E_1 \rightarrow E_1$	159.2	151.7		
	$E_2 \rightarrow E_2$	204.7	211.4				$E_2 \rightarrow E_2$	159.2	152.1		
	$E_3 \rightarrow E_3$	204.4	209.5				$E_3 \rightarrow E_3$	159.2	151.7		
	$E_4 \rightarrow E_4$	204.4	209.5				$E_4 \rightarrow E_4$	158.2	151.7		

[a]CCSD(T)/aug-cc-pVTZ frequencies. [b]Adjusted frequencies according to the text.[11] [c]In boldface are band energies assigned in ref 14, and in italic are band assignments proposed in this work. [d]Relative intensity obtained from eq 5 for the infrared absorption spectrum.

of transitions 010 → 020 and 030 → 040 have been calculated at around 217.3 and 210.6 cm^{-1} using the adjusted potential V^{ADJ}, while they have been observed at 218.1 and 210.6 cm^{-1}. For this reason, the unlabeled transition lines could be assigned for the first time, that is, the unassigned 020 → 030 transition corresponding to the ν_{20} mode has been computed at around 214.9 cm^{-1}. We propose to assign it to the band lying at 215.5 cm^{-1}. Also, the 001 → 011 splittings have been calculated to lie among 209.5 and 211.4 cm^{-1}. They can be assigned to the peaks observed at 209.8 and 211.4 cm^{-1}. We have predicted the positions for four more weak bands corresponding to excitations of the ν_{21} (400 → 500, 010 → 110, 110 → 210, and 001 → 101).

In the Raman spectrum, the two overtones $2\nu_{20}$ and $2\nu_{21}$ have been calculated at 448.8 and 318.2 cm^{-1} with the pure ab initio PES and at 442.8 and 316.1 cm^{-1} with the adjusted potential. These data confirm assignments to the bands observed at 442.0 and 316.5 cm^{-1}. The good agreement between observation and calculations has allowed us to propose the assignment of one band observed at 422.5 cm^{-1} to the 020 → 040 transition calculated at 424.5 cm^{-1}.

Two-Dimensional PESs. The aim of these series of papers focused on DME isotopologues is to help future experimental studies. For two-rotor problems, many experimental spectral studies are performed using 2D effective Hamiltonians depending on the torsional coordinates. In the case of DME, a 2D-PES can be useful for the two fundamental bands for which Fermi interactions with the COC-bending are negligible. However, to obtain empirically a 2D-PES is not easy for G_{36} species. For those, a unique torsional mode is infrared-active, and the only available experimental data corresponding to the second torsional mode is the position of the overtone in the

Table 7. Computed and Observed Raman Transitions of DME-d_3 (in cm^{-1})

	symm.	calc.[a]	adj.[b]	obs.[c]		symm.	calc.[a]	adj.[b]	obs.[c]
	$\nu\ \nu'\ \nu'' \rightarrow \nu\ \nu'+2\ \nu''$					$\nu\ \nu'\ \nu'' \rightarrow \nu+2\ \nu'\ \nu''$			
000 → 020	$A_1 \rightarrow A_1$	448.7	442.6	**442.0**	000 → 200	$A_1 \rightarrow A_1$	318.2	316.1	**316.5**
	$E_1 \rightarrow E_1$	448.8	442.8			$E_1 \rightarrow E_1$	318.2	316.1	
	$E_2 \rightarrow E_2$	448.7	442.6			$E_2 \rightarrow E_2$	318.2	316.1	
	$E_3 \rightarrow E_3$	448.8	442.8			$E_3 \rightarrow E_3$	318.2	316.1	
	$E_4 \rightarrow E_4$	448.8	442.8			$E_4 \rightarrow E_4$	318.2	316.1	
010 → 030	$A_2 \rightarrow A_2$	444.3	432.1	**435.0**	100 → 300	$A_2 \rightarrow A_2$	300.5	298.2	–
	$E_1 \rightarrow E_1$	444.5	431.2			$E_1 \rightarrow E_1$	300.4	298.2	
	$E_2 \rightarrow E_2$	444.2	431.1			$E_2 \rightarrow E_2$	300.3	298.0	
	$E_3 \rightarrow E_3$	444.5	432.1			$E_3 \rightarrow E_3$	300.3	298.0	
	$E_4 \rightarrow E_4$	444.6	431.1			$E_4 \rightarrow E_4$	300.3	298.0	
020 → 040	$A_1 \rightarrow A_1$	438.7	425.4	*422.5*	200 → 400	$A_1 \rightarrow A_1$	276.5	274.1	–
	$E_1 \rightarrow E_1$	442.8	424.5			$E_1 \rightarrow E_1$	276.6	274.1	
	$E_2 \rightarrow E_2$	438.7	425.3			$E_2 \rightarrow E_2$	278.0	275.6	
	$E_3 \rightarrow E_3$	440.4	427.7			$E_3 \rightarrow E_3$	277.9	275.6	
	$E_4 \rightarrow E_4$	442.1	427.4			$E_4 \rightarrow E_4$	278.0	275.6	
100 → 120	$A_2 \rightarrow A_2$	431.4	425.4	**426.0**	010 → 210	$A_2 \rightarrow A_2$	529.0	252.4	–
	$E_1 \rightarrow E_1$	429.5	425.7			$E_1 \rightarrow E_1$	529.5	257.3	
	$E_2 \rightarrow E_2$	431.4	425.4			$E_2 \rightarrow E_2$	529.5	248.6	
	$E_3 \rightarrow E_3$	429.5	425.7			$E_3 \rightarrow E_3$	529.0	257.8	
	$E_4 \rightarrow E_4$	429.5	425.7			$E_4 \rightarrow E_4$	529.0	257.7	
110 → 130	$A_1 \rightarrow A_1$	365.8	407.7	**397.0**	110 → 310	$A_1 \rightarrow A_1$	288.3	280.6	–
	$E_1 \rightarrow E_1$	366.3	406.3			$E_1 \rightarrow E_1$	289.7	283.3	
	$E_2 \rightarrow E_2$	366.4	406.6			$E_2 \rightarrow E_2$	288.5	280.8	
	$E_3 \rightarrow E_3$	365.7	405.5			$E_3 \rightarrow E_3$	289.8	283.5	
	$E_4 \rightarrow E_4$	365.7	405.7			$E_4 \rightarrow E_4$	289.8	283.5	
					$\nu\ \nu'\ \nu'' \rightarrow \nu\ \nu'\ \nu''+1$				
000 → 001	$A_1 \rightarrow A_1$	396.2	373.1	**373.0**	001 → 002	$A_1 \rightarrow A_1$	410.9	373.6	–
	$E_1 \rightarrow E_1$	396.2	373.1			$E_1 \rightarrow E_1$	413.7	373.4	
	$E_2 \rightarrow E_2$	396.2	373.1			$E_2 \rightarrow E_2$	413.9	373.6	
	$E_3 \rightarrow E_3$	396.2	373.1			$E_3 \rightarrow E_3$	413.6	373.4	
	$E_4 \rightarrow E_4$	396.2	373.1			$E_4 \rightarrow E_4$	413.4	373.4	
$\nu\ \nu'\ \nu'' \rightarrow \nu+1\ \nu'+1\ \nu''$									
000 → 110	$A_1 \rightarrow A_1$	379.8	382.4	**384.0**	110 → 220	$A_1 \rightarrow A_1$	344.6	325.5	–
	$E_1 \rightarrow E_1$	379.9	382.5			$E_1 \rightarrow E_1$	351.4	330	
	$E_2 \rightarrow E_2$	379.8	382.4			$E_2 \rightarrow E_2$	344.8	318.8	
	$E_3 \rightarrow E_3$	379.9	382.5			$E_3 \rightarrow E_3$	351.1	318.7	
	$E_4 \rightarrow E_4$	379.8	382.5			$E_4 \rightarrow E_4$	351.1	318.7	
010 → 120	$A_2 \rightarrow A_2$	367.4	361.8	**364.0**	100 → 210	$A_2 \rightarrow A_2$	366.0	377.8	**380.0**
	$E_1 \rightarrow E_1$	367.5	361.2			$E_1 \rightarrow E_1$	365.5	377.0	
	$E_2 \rightarrow E_2$	367.4	361.8			$E_2 \rightarrow E_2$	365.5	377.8	
	$E_3 \rightarrow E_3$	367.5	361.2			$E_3 \rightarrow E_3$	366.0	377.0	
	$E_4 \rightarrow E_4$	367.5	361.2			$E_4 \rightarrow E_4$	366.0	377.0	
020 → 130	$A_1 \rightarrow A_1$	296.9	347.5	**337.0**	200 → 310	$A_1 \rightarrow A_1$	349.9	346.9	–
	$E_1 \rightarrow E_1$	297.5	346.0			$E_1 \rightarrow E_1$	351.4	349.7	
	$E_2 \rightarrow E_2$	297.5	346.4			$E_2 \rightarrow E_2$	350.1	347.1	
	$E_3 \rightarrow E_3$	296.8	345.2			$E_3 \rightarrow E_3$	351.5	349.9	
	$E_4 \rightarrow E_4$	296.8	345.3			$E_4 \rightarrow E_4$	351.5	349.9	

[a]CCSD(T)/aug-cc-pVTZ frequencies. [b]Adjusted frequencies according to the text.[11] [c]In boldface are band energies assigned in ref 14; in italic are band assignments proposed in this work.

Raman spectrum. Unfortunately, this overtone is displaced by Fermi resonances.

For this reason, we have derived 2D effective potentials from our adjusted 3D effective surfaces. They are obtained determining the average value of the bending coordinate in the zero-point vibrational energy level. We obtain 111.3° for DME-h_6, 111.9° for DME-d_6, and 112.0° for DME-d_3. Using these values in the adjusted 3D-PES we obtain

$$V(\theta_1, \theta_2) = 939.00 - 475.12(\cos 3\theta_1 + \cos 3\theta_2) + 17.467 \cos 3\theta_1 \cos 3\theta_2 + 3.50(\cos 6\theta_1 + \cos 6\theta_2) - 0.56(\cos 3\theta_1 \cos 6\theta_2 + \cos 6\theta_1 \cos 3\theta_2) + 1.71 \cos 6\theta_1 \cos 6\theta_2 + 8.04 \sin 3\theta_1 \sin 3\theta_2, \quad \text{for DME-}h_6$$

$$V(\theta_1, \theta_2) = 927.50 - 471.54(\cos 3\theta_1 + \cos 3\theta_2) + 20.53 \cos 3\theta_1 \cos 3\theta_2 + 3.10(\cos 6\theta_1 + \cos 6\theta_2) - 0.35(\cos 3\theta_1 \cos 6\theta_2 + \cos 6\theta_1 \cos 3\theta_2) + 1.49 \cos 6\theta_1 \cos 6\theta_2 + 2.97 \sin 3\theta_1 \sin 3\theta_2, \text{ for DME-}d_6$$

$$V(\theta_1, \theta_2) = 930.71 - 468.64 \cos 3\theta_1 - 468.64 \cos 3\theta_2 + 21.78 \cos 3\theta_1 \cos 3\theta_2 + 3.55 \cos 6\theta_1 + 3.55 \cos 6\theta_2 - 0.52 \cos 3\theta_1 \cos 6\theta_2 - 0.52 \cos 6\theta_1 \cos 3\theta_2 + 2.04 \cos 6\theta_1 \cos 6\theta_2 - 7.48 \sin 3\theta_1 \sin 3\theta_2, \text{ for DME-}d_3$$

CONCLUSIONS

In this paper, a vibrationally corrected 3D-PES calculated for the analysis of DME-h_6 far-infrared spectra is employed to determine low vibrational energy levels of two deuterated species DME-d_3 and DME-d_6. The ab initio results as well as the levels calculated variationally from an adjusted PES are employed to discuss previous assignments of experimental spectra.

Symmetry groups are employed to reduce computational expenses and for level and splittings assignments. For DME-d_6, splitting components transform as A_i, E_i (i = 1−4), and G irreducible representations of the G_{36} groups, whereas for DME-d_3, they transform as A_1, A_2, E_1, E_2, E_3, and E_4 of the G_{18} group. For both species, below 800 cm^{-1}, splitting energy differences are in general lower than 0.1 cm^{-1}.

For DME-d_6, only a fundamental transition (ν_{15}, 000 → 010) is IR-active. CCSD(T) calculations place it at 192.8 cm^{-1}, close to experimental value of 188.6 cm^{-1}. In general, our calculations confirm previous assignments.[14] As the agreement between observation and calculations is good, we have proposed assignments for the combination band 110 → 120 and the "hot" 001 → 011 transitions. For DME-d_3, we have proposed assignments for several bands including the unassigned 020 → 030 transition.

Further infrared and Raman spectral recordings of higher accuracy would be welcome in order to work out the assignments of the transitions involving the torsional and COC-bending states.

AUTHOR INFORMATION

Corresponding Author

*E-mail: senent@iem.cfmac.csic.es.

Notes

The authors declare no competing financial interest.

†E-mail: rosa.dominguez@upm.es (R.D.-G.); miguel.carvajal@dfa.uhu.es (M.C.); mvv@xanum.uam.mx (M.V.).

ACKNOWLEDGMENTS

This work has been supported by the Ministerio de Educación of Spain, through Grants AYA2008-00446 (Plan Nacional I+D +I (2004-2007)) and FIS2011-28738-C02-02 and computing resources of CESGA. Also, this work is partly supported by the Andalusian Government (Spain) under Contract Number P07-FQM-03014 and by a joint project within of a frame CNRS (France) and CSIC (Spain) agreement (Code Number: 2011 FR0018). The authors are very grateful to Prof. Jon Hougen and Prof. Isabelle Kleiner by their useful comments along this work.

REFERENCES

(1) Schilke, P.; Bendford, D. J.; Hunter, T. R.; Lis, D. C.; Phillips, T. G. *Astrophys. J.* **2001**, *132*, 281.

(2) Snyder, L. E.; Buhl, D.; Schwartz, P. R.; Clark, F. O.; Johnson, D. R.; Lovas, F. J.; Giguere, P. T. *Astrophys. J.* **1974**, *191*, L79.

(3) Endres, C. P.; Drouin, B. J.; Pearson, J. C.; Müller, H. S. P.; Lewen, F.; Schlemmer, S.; Giesen, T. F. *Astron. Astrophys.* **2009**, *504*, 635.

(4) Fortman, S. M.; Medvedev, I. R.; Neese, C. F.; de Lucia, F. C. *Astrophys. J. Lett.* **2010**, *725*, L11.

(5) Durig, J. R.; Li, Y. S.; Groner, P. *J. Mol. Spectrosc.* **1976**, *62*, 159.

(6) Lovas, F. J.; Lutz, H.; Dreizler, H. *J. Phys. Chem. Ref. Data.* **1979**, *8*, 1051.

(7) Neustock, W.; Guarnieri, A.; Demaison, J.; Wlodarzak, G. *Z. Naturforsch. A: Phys. Sci.* **1990**, *45*, 702.

(8) Groner, P.; Albert, S.; Herbst, E.; de Lucia, F. C. *Astrophys. J.* **1998**, *500*, 1059.

(9) Coudert, L. H.; Çarçabal, P.; Chevalier, M.; Broquier, M.; Hepp, M.; Herman, M. *J. Mol. Spectrosc.* **2002**, *212*, 203.

(10) Guélin, M.; Brouillet, N.; Cernicharo, J.; Combes, F.; Wooten, A. *Astrophys. Space Sci.* **2008**, *313*, 45.

(11) Villa, M.; Senent, M. L.; Domínguez-Gómez, R.; Álvarez-Bajo, O.; Carvajal, M. *J. Phys. Chem. A* **2011**, *115*, 13573.

(12) Senent, M. L.; Moule, D. C.; Smeyers, Y. G. *Can. J. Phys.* **1995**, *73*, 425.

(13) Senent, M. L.; Moule, D. C.; Smeyers, Y. G. *J. Chem. Phys.* **1995**, *102*, 5952.

(14) Groner, P.; Durig, J. R. *J. Chem. Phys.* **1977**, *66*, 1856.

(15) Senent, M. L. *Chem. Phys. Lett.* **1998**, *296*, 299.

(16) Senent, M. L. *J. Mol. Spectrosc.* **1998**, *191*, 265.

(17) Smeyers, Y. G.; Senent, M. L.; Botella, V.; Moule, D. C. *J. Chem. Phys.* **1993**, *98*, 2754.

(18) Smeyers, Y. G.; Bellido, M. N. *Int. J. Quantum Chem.* **1981**, *19*, 553.

(19) Carvajal, M.; Álvarez-Bajo, O.; Senent, M. L.; Domínguez-Gómez, R.; Villa, M. *Chem. Phys.* **2012**, inpreparation.

(20) Scuseria, G. E.; Schaefer, H. F., III. *J. Chem. Phys.* **1989**, *90*, 3700.

(21) Pople, J. A.; Head-Gordon, M.; Raghavachari, K. *J. Chem. Phys.* **1987**, *87*, 5968.

(22) Woon, D. E.; Dunning, T. H., Jr. *J. Chem. Phys.* **1993**, *98*, 1358.

(23) Frisch, M. J.; Trucks, G. W.; Schlegel, H. B.; Scuseria, G. E.; Robb, M. A.; Cheeseman, J. R.; Scalmani, G.; Barone, V.; Mennucci, B.; Petersson, G. A.; et al. *Gaussian 09*, revision A.1; Gaussian, Inc.: Wallingford, CT, 2009.

(24) (a) Senent, M. L. *ENEDIM*, A variational code for non-rigid molecules. http://tct1.iem.csic.es/senent/PROGRAMAS.htm (2001). (b) Senent, M. L. *FIT-ESPEC*, A Fortran code for calculating spectroscopic parameters from a force field in internal coordinates. http://tct1.iem.csic.es/senent/PROGRAMAS.htm (2007).

(25) Senent, M. L. *Mol. Phys.* **2001**, *99*, 1311.

(26) Senent, M. L. *J. Phys. Chem. A* **2004**, *108*, 6286.

(27) Senent, M .L.; Villa, M.; Meléndez, F. J.; Domínguez-Gómez, R. *Astrophys. J.* **2005**, *627*, 567.

(28) Senent, M. L.; Moule, D. C.; Smeyers, Y. G. *J. Phys. Chem.* **1995**, *99*, 7970.

(29) Moule, D. C.; Smeyers, Y. G.; Senent, M. L.; Clouthier, D. J.; Karolczak, J.; Judge, R. *J. Chem. Phys.* **1991**, *95*, 3137.